Tr. J. of Physics
23 (1999) , 1031 – 1039.

Implications of $\Delta\rho$ and Charm II data for Z′ Physics

D. A. DEMİR*
Middle East Technical University, Department of Physics,
06531, Ankara-TURKEY

Received 27.01.1999

Abstract

We discuss the constraints on the Z' model parameters coming from Z-pole and low-energy $\nu_\mu - e$ scattering data in the frame work of GUT-motivated models. We find that when the coupling constant of the extra $U(1)$ is small (large) the parameter space is mainly determined by the Z-pole (the low-energy $\nu_\mu - e$ scattering) data.

Introduction

Deviations of the precisely measured electroweak observables from the predictions of the SM [1] enable one to search for the existence of new physics. Although there are various possibilities for extending the SM, one of the simplest and well-motivated extension is the addition of an extra $U(1)$ to its $SU(3)_C \times SU(2)_L \times U(1)_Y$ gauge structure [2]. The Z-pole and neutral current data can be used to search for and set limits on the existence of the Z' models [3]. The Z-pole observables are sensitive only to the $Z - Z'$ mixing angle due to the modifications in the vector and axial couplings of the fermions to the Z-boson. On the other hand, off-Z-pole $e^+ - e^-$ data, and low energy $\nu_\mu - e, v$-hadron and parity-violating e-hadron scattering experiments are sensitive to both $Z - Z'$ mixing and Z' mass [3]. Therefore, accompanying the Z-pole data, the low-energy observables are particularly useful in establishing the constraints on the Z' physics. For example, atomic parity violation experiments (particularly for cesium) has already been analyzed in this direction [4, 5].

In this work we investigate the implications of $\Delta\rho$ and CHARM II data [6] on the Z' models by comparing them with the SM predictions [7, 8, 9]. In the analysis, we illustrate two GUT-motivated models and reach conclusions of general applicability.

In Sec. 2 we give the relevant formulae for the effective vector and axial couplings in the frame work of the Z' models. Moreover, we list SM expressions and derscribe the

*e-mail:ddemir@ictp.trieste.it Present Address: ICTP, Trieste, Italy

GUT-motivated Z' models that will be the subject matter of the analysis.

In Sec. 3 we a detailed numerical analysis of the appropriate parameter space by taking into account both points implied by the CHARM II data [6].

In Sec. 4 we conclude the work and remark on the interplay between low-energy and Z-pole determinations of the parameter space.

$\mathbf{V}_\mu - e$ Scattering in Z′ Models

In addition to the usual SM gauge group, we consider an additional Abelian group $U(1)_{Y\prime}$ with coupling constant $g_{Y\prime}$, under which the left-handed lepton doublets and right-handed charged leptons have charges Q_L and Q_E, respectively. The neutral vector bosons Z of $SU(2)_L \times U(1)_Y$ and Z' of $U(1)_{Y\prime}$ mix with each other. The mass eigenstate vector bosons Z_1 and Z_2 can be obtained after diagonalizing the $Z - Z'$ mass-squared matrix:

$$Z_1 = Z\cos\theta + Z'\sin\theta, \tag{1}$$
$$Z_2 = -Z\sin\theta + Z'\cos\theta, \tag{2}$$

which define the $Z - Z'$ mixing angle θ. The Z' effects can show up in various physical quantities whose comparison with the SM predictions allow us to constrain Z' parameters in a model-independent way. In general, Z' effects can be tracked by their apprearence in four distinct physical quantities. Firstly, due to mixing, Z_1 is lighter than the canonical Z, so that the ρ parameter predicted by Z_1 mass is larger than the one predicted by Z mass. Secondly, coupling of Z_1 to fermions differs from those of Z due to the mixing in (1). Thirdly, the Z_1 exchange will modify the neutral current amplitudes as an explicit function of the Z' mass. Finally, $\sin^2\theta_w$ differs from the SM prediction because of the Z' contribution to the ρ parameter. In what follows we shall discuss all of these effects in the framework of $\mu_\mu - e$-scattering.

The low-energy four-fermion effective lagrangian relevant to $\nu_\mu - e$-scattering can be written as

$$-L^{\nu_\mu - e} = \frac{G_F}{\sqrt{2}}\bar{\nu}_\mu\gamma^\alpha(1-\gamma^5)\nu_\mu\bar{e}\gamma_\alpha(g_V^{\nu_\mu e} - g_A^{\nu_\mu e}\gamma^5)e, \tag{3}$$

which defines the effective vector coupling $g_V^{\nu_\mu e}$ and axial coupling $g_V^{\nu_\mu e}$. $\nu_\mu - e$ scattering is a pure neutral current process mediated by both Z_1 and Z_2. Thus $g_V^{\nu_\mu e}$ and $g_A^{\nu_\mu e}$ carry the Z' effects through the contribution of the termediate vector bosons, and the modification of the fermion-vector boson couplings due to mixing. In the Z' model mentioned-above these couplings are given by the following:

$$\begin{aligned} g_V^{\nu_\mu e} &= \rho_1\{\tilde{g}_V^{\nu_\mu e}\cos^2\theta + \lambda(1+r+2\tilde{g}_V^{\nu_\mu e})\sin 2\theta + 8\lambda^2(1+r)\sin^2\theta\} \\ &\quad + \rho_2\{\tilde{g}_V^{\nu_\mu e}\sin^2\theta\lambda(1+r+2\tilde{g}_V^{\nu_\mu e})\sin 2\theta + 8\lambda^2(1+r)\cos^2\theta\} \\ g_A^{\nu_\mu e} &= \rho_1\{\tilde{g}_V^{\nu_\mu e}\cos^2\theta + \lambda(1-r+2\tilde{g}_V^{\nu_\mu e})\sin 2\theta + 8\lambda^2(1-r)\sin^2\theta\} \end{aligned} \tag{4}$$

$$+ \rho_2\{\tilde{g}_V^{\nu_\mu e}\sin^2\theta - \lambda(1-r+2\tilde{g}_A^{\nu_\mu e})\sin 2\theta + 8\lambda^2(1-r)\cos^2\theta\}. \quad (5)$$

Here, ρ_1 and ρ_2 are the ρ parameters of Z_1 and Z_2:

$$\rho_1 = \frac{1+\eta^2\tan^2\theta}{1+\tan^2\theta} \quad (6)$$

$$\rho_2 = \frac{1+\eta^2\tan^2\theta}{\eta^2(1+\tan^2\theta)}, \quad (7)$$

where $\eta = M_{z2}/M_{z1}$. Next, $\lambda = (g_{Y\prime}Q_L)/(2G)$, $r = Q_E/Q_L$, and $G = \sqrt{g_2^2+g_Y^2}$. Finally, the tilded vector and axial couplings are given by

$$\tilde{g}_V^{\nu_\mu e} = (g_V^{\nu_\mu e})_{SM} - 2(\frac{S_W^2 C_W^2}{C_W^2 - S_W^2})SM\Delta\rho \quad (8)$$

$$\tilde{g}_A^{\nu_\mu e} = (g_A^{\nu_\mu e})_{SM}, \quad (9)$$

where the subscript SM refers to the SM value of the associated quantity. Here $\Delta\rho$ is the deviation of the ρ_1 from its SM value:

$$\Delta\rho = \rho_1 - 1 = (\eta^2 - 1)\sin^2\theta. \quad (10)$$

It is the Z' contribution to S_W^2 that causes a finite difference between $\tilde{g}_V^{\nu_\mu e}$ and $(g_V^{\nu_\mu e})_{SM}$. As we see the Z' contribution to S_W^2 is proportional to $\Delta\rho$.

We identify $(g_V^{\nu_\mu e})_{SM}$ in (4) and $(g_A^{\nu_\mu e})_{SM}$ in (5) with the experimental result, and require the Z' contributions at their right hand sides to close the gap between experimental result and the SM determination. We use the SM results evaluated for $M_H = M_Z$ so that there is no contribution to a particular observable from the Higgs loop. This is a convenient approach as we have a much more complicated Higgs sector in Z' models (See, for example, [10] and references therein) with increased number of scalars whose contributions to a particular observable differ from the one in SM. Moreover, the tree-level Z' contributions in 54) and (5) do already yield the relevant parameters of a Z' model to be fixed at the leading order. Namely, we assume loop corrections to (4) and (5) coming from the Z' sector are negligably small.

Although we treat Z' effects at the tree-level, we take all the loop contributions into account when analyzing the SM contribution. One of the basic SM parameters entering (4) and (5) is the weak mixing angle S_W^2 whose meaning is to be fixed against the ambiguities coming from the renormalization scheme and scale. As was discussed in [1] in detail, the value of S_W^2 extracted from M_z in $\bar{M}\bar{S}$ scheme at the scale M_z is less sensitive to m_t and most types of the new physics compared to the others. Following [1], we adopt this definition of S_W^2 to be denoted by $\hat{s}_Z^2$ from now on. Consistent with this choice for S_W^2, the SM expressions for vector and axial couplings in (8) and (9) are given by

$$(g_V^{\nu_\mu e})_{SM} = p_{ve}(-1/2 + 2\hat{K}_{ve}\hat{s}_Z^2) \tag{11}$$
$$(g_A^{\nu_\mu e})_{SM} = p_{ve}(-1/2) \tag{12}$$

whose numerical values can be found in [1].

In the analysis below we shall restrict η and θ by requiring (4) and (5) be satisfied within the experimental error bounds. In addition to this, we take into account the constraints coming from Z-pole data by requiring $\Delta\rho$ (10) be in the band induced by the present world average for ρ_1 [1]:

$$0.999 \leq \rho_1 \leq 1.0006, \tag{13}$$

which puts an additional restriction on the allowed $\eta - \theta$ space. $\Delta\rho$ calculated from (13) includes m_t effects already; however, Higgs effects are discarded by taking $M_H = M_Z$, as mentioned before. Although $\Delta\rho = \rho_1 - 1$ takes both negative and positive values, Z' models require it be positive as M_{Z_1} is less than M_Z due to mixing.

The lepton charges Q_L and Q_E and gauge coupling $g_{Y\prime}$ are model dependent. In literature there are various Z' models [5] with definite predictions for charges and gauge coupling. In this work we shall illustrate the constraints implied by CHARM II results by considering two typical GUT-motivated Z' models. Obviously, when choosing the models one should discard those that predict a right-handed neutrino as the form of the effective lagrangian (3) suggests.

The first model is the I model coming from E_6 [2, 11], and we call it Model $\mathcal{B}$. In this model $Q_L = -2Q_E = 1/\sqrt{10}$ and $g_{Y\prime} \simeq 0.8g_2$. This is a typical E_6- inspired model in which $U(1)_{Y\prime}$ charges are linear combinations of the $U(1)$ groups $E_6/SO(10)$ and $SO(10/SU(5)$. Depending on the details of the symmetry breaking, $g_{Y\prime}$ differs from $0.8g_2$ by a factor around unity.

The second model we analyze is the one following from the breaking of the flipped $SU(5)\times U(1)$ when the Higgs fields reside in the $(27+\bar{27})dimensionalrepresentationofE(6)$ [2, 11]. In this model $Q_L = Q_E = 1/2$ and $g_{Y\prime}$ is as in the first model. We call this model as Model $\mathcal{A}$.

In the notation of equations (4) and (5), we have $r_{\mathcal{A}} = 1, r_{\mathcal{B}} = -1/2$ and $\lambda_{\mathcal{A}} \simeq 0.63\lambda_{\mathcal{A}}$. Since $r_{\mathcal{A}} = 1, g_A^{\nu_\mu e}$ feels Z' parameters only through $\lambda \sin 2\theta$ type terms (see (5)) which is a weaker dependence than that of $g_V^{\nu_\mu e}$. Thus, in Model $\mathcal{A}$ parameter space is expected to be constrained mainly by $\Delta\rho$ and $g_A^{\nu_\mu e}$.

In Model $\mathcal{B}$, as $r_{\mathcal{B}} = -1/2$, dependence of $g_A^{\nu_\mu e}$ on Z' parameters is amplified compared to $g_A^{\nu_\mu e}$. Thus, one excepts $\Delta\rho$ and $g_A^{\nu_\mu e}$ mainly determine the appropriate parameter space.

Finally, one can also predict the relative magnitudes of the parameter spaces in two models. Since $\lambda_{\mathcal{B}} \simeq 0.63\lambda_{\mathcal{A}}$, it is clear that in Model $\mathcal{B}$ one needs a wider parameter space than in Model $\mathcal{A}$ to close the gap between experiment and the SM. In the next section we shall quantify these qualitative arguments.

CHARM II Results and Z′ Physics

CHARM II Collaboration [6] has measured S_W^2, $g_V^{\nu_\mu e}$ from the neutrino-electron scattering events using ν and $\bar{\nu}$ beams with $E_\nu \sim 25.7GeV$. On the $gv - g_A$ plane there are two candidate points coming from electron-neutrino scattering data. However, LEP results for $A_{FB}(e^+e^- \to e^+e^-)$ [13] prefer one of them, at which $g_V^{\nu_\mu e}$=-0.035±0.017 and $g_A^{\nu_\mu e}$=-0.503±0.017 [1]. This solution, which we call point (I), is close to the SM prediction so that it can be taken as a confirmation of the standard electroweak theory. The other point, which is discarded by e^+e^- data, is approximately given by $g_V^{\nu_\mu e} \leftrightarrow g_A^{\nu_\mu e}$. This solution, which we call point (II), is clearly far from being predictable by the SM. As noted in [1], point (I) is choosen by assuming that the Z-pole data is dominated by a single Z. In multi Z models, like the Z' models under concern, it would be convenient to discuss the implications of both points for Z' physics on equal footing. Below we first analyze the allowed parameter space on $\eta - \theta$ plane for the point (I), then we turn to the discussion of point (II).

Allowed $\eta - \theta$ values for point (I)

Let us start discussing the implications of equations (4), (5), and (10) with a rough analysis. Equations (4) and (5) express experimental values of $g_V^{\nu_\mu e}$ and $g_A^{\nu_\mu e}$ in terms of the parameters of the extended model at hand. Equation (10), on the other hand, represents the restriction on the modification of ρ parameter due to Z' effects. As given in (13), $\Delta\rho$ (10) is restricted in a rather narrow error band. As is seen from equations (4)-(9), $g_V^{\nu_\mu e}$ and $g_A^{\nu_\mu e}$ explicitly depend on $\Delta\rho$, unlike the atomic weak charge for which $\Delta\rho$ dependence almost cancel [5].

For a rough analysis of the parameter space at point (I), one can neglect $\Delta\rho$ all together. Then $\tilde{g}_V^{\nu_\mu e}$ (8) reduces to the SM expression. More-over, $\rho_1 \to 1$, and this requires both $\eta^2 \tan^2\theta$ be small, which would be satisfied only by a small enough θ. That $g_V^{\nu_\mu e}$ and $g_A^{\nu_\mu e}$ are close to their SM values also confirms the need for a small θ, as this reduces the ρ_1 dependent terms in (4) and (5) essentially to their SM expressions. In this limit, $\rho_2 \sim 1/\eta$, and for $\rho_2 \cos^2\theta$ type terms in (4) and (5) being suppressed, one needs a large η or, equivalently, heavy enough Z_2. After making these rough observations we now turn to an exact numerical analysis of the allowed $\eta - \theta$ region for point (I), which will be seen to imply constraints beyond these expectations as one considers the nonvanishing values of the ρ parameter.

In the numerical analysis below we first express, via (10), η in terms of θ for a given value of $\Delta\rho$. Then we insert this solution to the expressions for $g_V^{\nu_\mu e}$ and $g_A^{\nu_\mu e}$ in (4) and (5). After expressing (4) and (5) in terms of θ and $\Delta\rho$ in this way we let θ vary from zero to higher values; meanwhile, $\Delta\rho$ wanders in its phenomenologically allowed range of values determined by (13). Under the variation of these parameters we pick up those points for which (4) and (5) do remain in their allowed range of values.

We first analyze Model $\mathcal{A}$ mentioned in the last section. In this model $g_A^{\nu_\mu e}$ has a weaker dependence on the Z' parameters compared to $g_V^{\nu_\mu e}$ since r=1. Figure 1 depicts the allowed parameter space for which (4), (5) and (10) satisfy the existing phenomenological

bounds. As we see from Fig. 1 for small $\theta\eta$, wanders in a rather wide range of values. For example, for $\theta = 10^{-4}\pi, \eta$ varies fro 8 to 80, which implies $0.7TeV \leq_\sim M_{Z_2} \leq_\sim 7TeV$. As θ increases, not only the upper bound but also the lower bound on η decreases. For example, for $\theta \approx 0.0041\eta$, ranges from 1.3 to 6, that is, 120 $GeV \leq_\sim M_{Z_2} \leq_\sim 550GeV$, therefore Z_2 is considerably light in this case. Moreover, as θ increases further, the allowed range of η gets thinner and thinner and M_{z_2} settles approximately to 120 GeV. This goes on until $\theta = 0.0286$ at which $g_V^{\nu_\mu e}$ hits its lower bound, and there are no (θ, η) pairs satisfying (4), (5) and (10) beyond this point. In sum, one concludes that for Model $\mathcal{A}$, $\theta_{max} = 0.0286$ and $M_{z_2}^{min} \approx 120GeV$. For negative θ values, graph is approximately mirror symmetric of Fig. 1 with respect to η axis. θ takes its minimum value of $\theta_{min} = -0.236$ at which $g_V^{\nu_\mu e}$ reaches its upper bound. Close to θ_{min}, η drops to ~ 1.1, yielding a light Z_2.

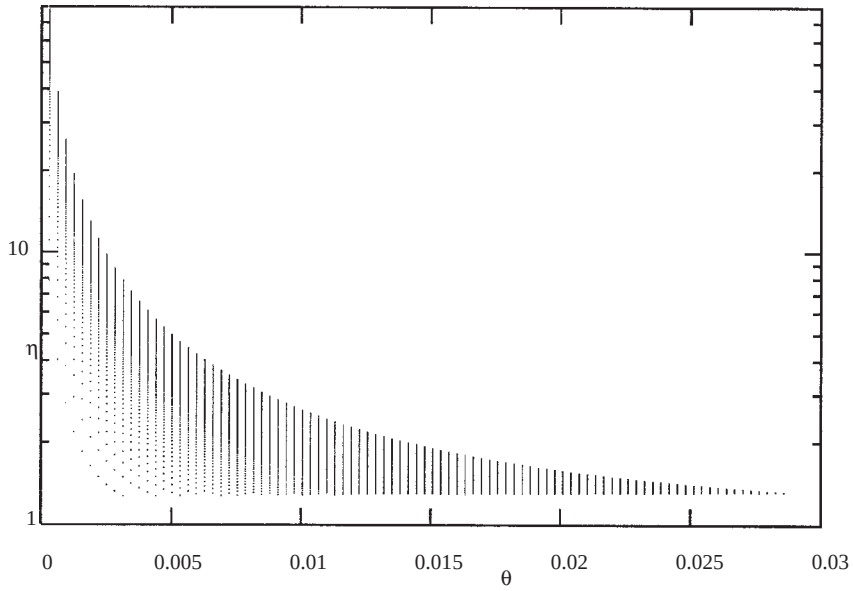

Figure 1. The $(\eta, theta)$ values satisfying (4), (5) and (10) for Model $\mathcal{A}$.

Now we analyze Model $\mathcal{B}$ to indentify the appropriate region it implies in the (θ, η) plane. As we recall from the previous section, unlike Model $\mathcal{A}$, in this model both $g_A^{\nu_\mu e}$ is more sensitive to the $g_V^{\nu_\mu e}$. Figure 2 depicts the appropriate (θ, η) pairs for which (4), (5) and (10) reside in their allowed band of values. Here we show only $\theta \geq 0.2$ part of the entire θ range to magnify the region of maximum θ value. $\theta \leq 0.2$ part behaves similarly to Fig. 1. As we see from Fig. 2, the allowed range of θ is rather wide compared to Model $\mathcal{A}$. This is what was expected by the discussions at the end of the last section. To be quantitave let us discuss some special points on Fig. 2. Here $\theta_{max} = 0.3896$ at which $g_A^{\nu_\mu e}$ hits its upper bound so that there is no acceptable (θ, η) values beyond this point. Consistent with the comperatively large values of θ, η takes its smallest allowed value,

that is, it takes the value of unity for every θ allowed, including the $\theta \leq 0.2$ part not shown on Fig. 2. For negative θ values the allowed region is approximately symmetric to Fig. 2 with respect to η axis and extends up to -1.533 at which $g_A^{\nu_\mu e}$ reaches its upper bound. Different from the positive θ range, η does not take the value of unity altough it remains close to unity, lowering as low as 1.005 for θ values near $\theta_{min} = -1.533$.

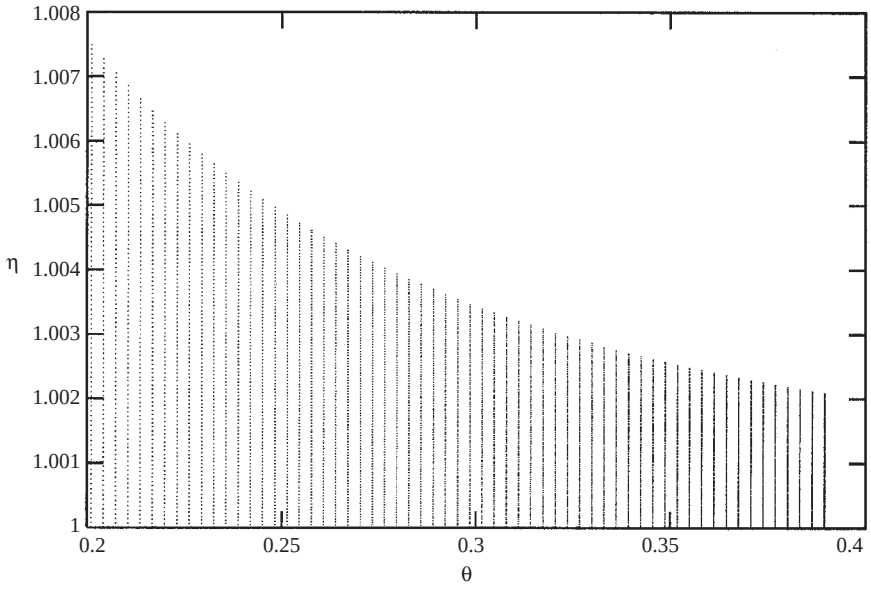

Figure 2. The $(\eta, theta)$ values satisfying (4), (5) and (10) for Model $\mathcal{B}$.

Although $\eta = 1$ was never realized for Model $\mathcal{A}$, it is the case here. This shows that for Model $\mathcal{B}$ the envelope of the allowed (θ, η) values is strictly determined by $\Delta\rho$ in (10), as $\eta = 1$ is consistent with the $\Delta\rho$ constraint. For Model $\mathcal{A}$, however, $\Delta\rho$ has not the full control over η values for a given θ, in that other parameters, $g_V^{\nu_\mu e}$ $g_A^{\nu_\mu e}$, constrain the total η range.

For both models $\mathcal{A}$ and $\mathcal{B}$ we have a wider range of allowed negative θ values which stems from the fact that negative θ changes the sign of the cross terms in (4) and (5), and thus, lowers the value of the right hand side compared to the positive θ case. This then requires a wider range of θ values. This widening of the allowed negative θ interval is also seen in the APV determination of [5]. However, one notes that, in general, the allowed ranges of θ is much wider than those of the APV determination. Nevertheless, a direct comparison is not possible, because in [5], experimental data are taken with an error of two standard deviations, and top mass is assigned a much lower value of ~ 90 GeV than the present analysis.

We conclude this subsection by noting that the allowed ranges of the mixing angle and Z_2 mass depend on the value of the normalized $U(1)_{Y'}$ coupling λ. If it is small, mainly the Z-pole observable $\Delta\rho$ takes control of the Z' parameter space, and the low-energy

observables $g_V^{\nu_\mu e}$ and $g_A^{\nu_\mu e}$ do not hit their phenomenological bounds until the mixing angle takes relatively large values. On the other hand, when λ is large, the low-energy observables become more decisive on the Z' parameter space. Therefore, one rhoughly concludes that when the coupling constant of the extra $U(1)$ is large (small) compared to the weak coupling low-energy observables (Z-pole observables) determine the allowed parameter space.

Allowed $\eta - \theta$ values for point (II)

In Sec. 3.1 we have discussed the implications of CHARM II candidate, point (I), for the Z' parameters. The other candidate, point (II), discarded by the e^+e^- data, deserves also a discussion because it may be of interest in Z' models in which off- Z, pole data may be explained by the contribution of the Z' propagator effects. Before an attempt to confirm the e^+e^- data, one should first prove the existence of points on the (θ, η) plane solving (4), (5) and (10) simultaneously. The transition from the point (I) to point (II) involves the exchange $g_A^{\nu_\mu e} \leftrightarrow g_A^{\nu_\mu e}$. Thus, it is convenient to work with $\sum^{\nu_\mu e} = g_V^{\nu_\mu e} + g_A^{\nu_\mu e}$ and $\Delta^{\nu_\mu e} = g_V^{\nu_\mu e} + g_A^{\nu_\mu e}$ which are symmetric and antisymmetric under $g_A^{\nu_\mu e} \leftrightarrow g_A^{\nu_\mu e}$, respectively. After interchanging the left hand sides of (4) and (5), $\sum^{\nu_\mu e}$ and $\Delta^{\nu_\mu e}$ can be expressed in terms of the corresponding SM ones and the other parameters. However, an attempt to find a consistent solution of $\sum^{\nu_\mu e}, \Delta^{\nu_\mu e}$ and $\Delta\rho$ for a given model parameters runs into difficulty immediately. This can be seen as follows. $\Delta^{\nu_\mu e}$ is symmetric under $g_V^{\nu_\mu e} \leftrightarrow g_A^{\nu_\mu e}$ so it points to the (θ, η) regions we discussed in Sec. 3.1. However, $\Delta^{\nu_\mu e}$ is antisymmetric under $g_V^{\nu_\mu e} \leftrightarrow g_A^{\nu_\mu e}$ and requires a completely different (θ, η) set for being satisfied. This is due to the fact that $\Delta^{\nu_\mu e}$ and the corresponding SM quantity Δ^{SM} are not as close to each other as $\sum^{\nu_\mu e}$ and $\sum^{SM}$. In fact, a numerical analysis of not only the models we have illustrated in Sec. 3.1 but also the ones listed in [5] confirms this observation. It is interesting that the present analysis also prefers the CHARM II result for point (I).

Conclusions

In this work we have analyzed the low energy $\nu_\mu - e$ scattering and Z-pole data against a general Abelian extension of the SM. In our analysis we have used the results of CHARM II Collaboration [6] which reported two candidate points for the effective vector and axial couplings. We have considered both points in our analysis and found that the CHARM II candidate discarded by the e^+e^- data does not lead a consistent solution for the GUT-motivated models considered. The other point, which is in the close vicinity of the SM predictions for effective vector and axial couplings, leads solution spaces much wider than the APV determination of [5]. The analysis concludes that when the gauge coupling associated to the extra $U(1)$ is small (large) compared to the weak coupling parameter space is determined mainly by ρ-parameter constraint (low-energy neutral current data).

References

[1] J. Erler and P. Langacker, in PDG 1997 Review, available at PDG WWW Pages (URL: http://pdg.lbl.gov/).

[2] J. Hewett, T. Rizzo, Phys. Rep. 183 (1989) 193.

[3] P. Langacker, M. Luo, and A. K. Mann, Rev. Mod. Phys. 64 (1992) 87.

[4] W. J. Marciano, J. L. Rosner, Phys. Rev. Lett. 65 (1990) 2963.

[5] K. T. Mahanthappa, P. K. Mohapatra, Phys. Rev. D 43 (1991) 3093, (E) 44 (1991) 1616.

[6] P. Vilain et. al., CHARM II Collab., Phys. Lett. B 335 (1994) 246.

[7] V. A. Novikov, L. B. Okun, M. I. Vysotky, Phys. Lett. B 298 (1993) 453; Mod. Phys. Lett. A8 (1993) 2529, (E) A8 (1993) 3301.

[8] ALEPH, DELPHI, L3, OPAL, and The LEP Electroweak Working Group, CERN/PPE/93-157, Aug. 1993.

[9] T. M. Aliev, D. A. Demir, E. Iltan, J. Phys. G: Nucl. Part. Phys. 21 (1995) 1307.

[10] M. Cvetic, D. A. Demir, J. R. Espinosa, L. Everett, P. Langacker, Phys. Rev. D56 (1997) 2861.

[11] D. E. Brahm, L. J. Hall, Phys. Rev. D 41 (1990) 1067.

[12] K. T. Mahanthappa, P. K. Mohapatra, Phys. Rev. D 42 (1990) 1732.

[13] The LEP Collaborations: ALEPH, DELPHI, L3 and OPAL, Phys. Lett. B 276 (1992) 247.

[14] F. Abe et. al., CDF Collab., Phys. Rev. Lett. 79(1997) 2191.